Mechanobiology of Endothelial Cells Related to the Formation of Arterial Disease

8

Noriyuki Kataoka

Abstract

Atherosclerosis is a serious disease that causes cardiovascular diseases such as cerebral infarction and myocardial infarction. Endothelial cell injury is the first step in atherogenesis by inducing increase in the production of chemoattractant proteins and adhesion molecules to leukocytes (Ross, Nature 362 (6423): 801–809, 1993). One of the key events in atherogenesis is the recruitment of blood leukocytes, especially monocytes, to proatherogenic vascular regions (Swirski et al, J Clin Invest 117:195–205, 2007; Tacke et al, J Clin Invest 117:185–194, 2007) and their subsequent transmigration across endothelial cells. Interactions between leukocytes and endothelial cells involve multi-step processes including rolling, adhesion, locomotion, and transmigration. Therefore, mechanics and dynamics of endothelial cells and monocytes are important matters to understand the whole process of atherogenesis. Here, we show and discuss the mechanobiology of endothelial cells related to the formation of arterial disease.

Keywords

Atherogenesis • Endothelial cell • Monocyte • Mechanobiology

N. Kataoka (✉)
Department of Mechanical Engineering, College of Engineering, Nihon University, 1 Nakagawara, Tokusada, Tamuramachi, Koriyama, Fukushima, Prefecture Japan, 963-8642
e-mail: kataoka@mech.ce.nihon-u.ac.jp

K. Tanishita, K. Yamamoto (eds.), *Vascular Engineering*,
DOI 10.1007/978-4-431-54801-0_8

8.1 Changes in Micromechanics of Endothelial Cells Induced by Monocyte Adhesion

8.1.1 Measurement Tools of Micromechanics of Endothelial Cells

When monocytes migrate into the intima, endothelial cells might dynamically change their shape and cytoskeletal structure. It is considered that the endothelial cell micro-mechanics that are involved in the endothelial cell micro-motion and the mechanical properties of endothelial cells are important in these processes. For the micro-motion measurement of the cultured cells, Giaever and Keese (1991) developed a morphological biosensor named "Electric Cell-substrate Impedance Sensing (ECIS) system". In this system, we can detect the change of the electrical impedance that reflects the apposition of the cells to each other and to their substrate grown on the small gold electrode. The advantage of this system is that quantitative estimation of cell-to-cell and cell-to-substrate distances can be performed separately and in real time.

Atomic force microscope (AFM) is a useful tool not only for imaging the biological tissues but also for examining mechanical properties of cells. The measurement of mechanical properties of living soft tissue is possible with a nanoindentation technique (Radmacher et al. 1996). We applied these two methods, ECIS and AFM, to evaluate the effect of the interaction between monocyte and endothelial cell on the endothelial cell micro-motion and mechanical properties (Kataoka et al. 2002).

8.1.2 Estimation of Endothelial Cell-to-Cell and Cell-to-Substrate Gaps

Human umbilical vein endothelial cells (HUVECs) were seeded on a cell culture dish (10 mm × 10 mm for each section; Applied Biophysics, Inc., NY, USA) with a micro-electrode ($\phi = 250$ μm) (Fig. 8.1). HUVEC were then stimulated with interleukin-1β (5 ng/ml) 6 h and subsequently overlayered with the 20 μl of culture medium containing THP-1 cells that is a human monocytic cell line. The electrical impedance was measured with ECIS (Applied Biophysics, Inc.). The change of impedance is attributed to the changes of the resistance in paracellular pathway (Rb) and the resistance between the ventral cell surface and the electrode (α: $\alpha = r(r/h)^{0.5}$; r, cell radius; r, the resistivity of the culture medium; h, the gap between the cells and the electrode). From the changes of Rb and a, the changes in cell-to-cell and cell-to-substrate gaps were estimated.

8.1.3 Measurement of Mechanical Property Endothelial Cells

By pressing the AFM cantilever to the cell surface, a force-curve, the relationship between the cantilever deflection and its indentation depth, was obtained. In this study, the force curve of the HUVEC was measured with AFM (NVB100;

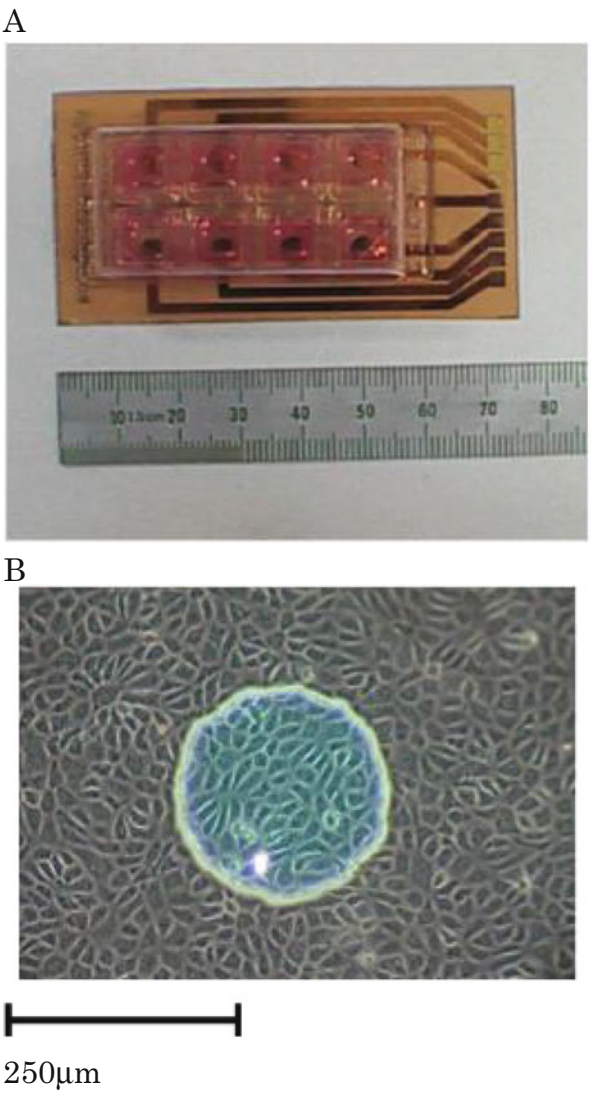

Fig. 8.1 (**a**) Cell culture dish for Electric Cell-substrate Impedance Sensing (ECIS) system, (**b**) Micro-electrode ($\phi = 250$ μm) covered with cultured endothelial cells in the center of the cell culture dish for ECIS

Olympus, Tokyo, Japan). HUVECs were seeded on a gelatin-coated cell culture dish, and THP-1 was applied. The force curves were measured after 2 h of application of THP-1 to HUVECs. Force-curve measurements were performed in the center region, just above the cell nucleus and the peripheral region of HUVEC. Elastic modulus was estimated with the Hertz model that describes the indentation of a homogeneous/semi-infinite elastic material (Radmacher et al. 1996).

$$F = \delta^2 \frac{\pi}{2} \frac{E}{(1 - v^2)} \tan \alpha$$

where F is the applied force (calculated from the spring constant multiplied by the cantilever deflection), E is the elastic modulus, v is the Poisson's ratio assumed to be 0.5, α is the opening angle of the tip of the cantilever, and δ is the indentation depth.

8.1.4 Results of Changes of Endothelial Cell Micromechanics

Typical traces of the total, cell-to-cell (Rb) and cell-to-substrate (α) resistances in the IL-1β stimulated HUVECs, are shown in Fig. 8.2. Immediately after the application of THP-1 cells (time = 0 in the figure) to the IL-1β stimulated HUVECs, cell-to-substrate resistance gradually decreased, whereas cell-to-cell resistance was almost unchanged. After 1 h of application of THP-1, α was significantly decreased by –40.1 ± 20.1 %, while the change in Rb was not significant (14.9 ± 50.6 %). At this stage, THP-1 adhered on the EC surface, but did not migrate into the EC monolayer.

Typical force curves for the peripheral region of the control HUVEC and the THP-1 adhered HUVEC are shown in Fig. 8.3. The changes of the elastic modulus in both the center and peripheral regions are shown in Fig. 8.4. Under the control condition, the elastic modulus in the central region was significantly smaller than that in peripheral region. The elastic modulus of the monocytes adhered HUVECs significantly decreased in both the central and peripheral regions. Coincidentally, the density of actin filaments and the number of $p125^{FAK}$ decreased (Fig. 8.5).

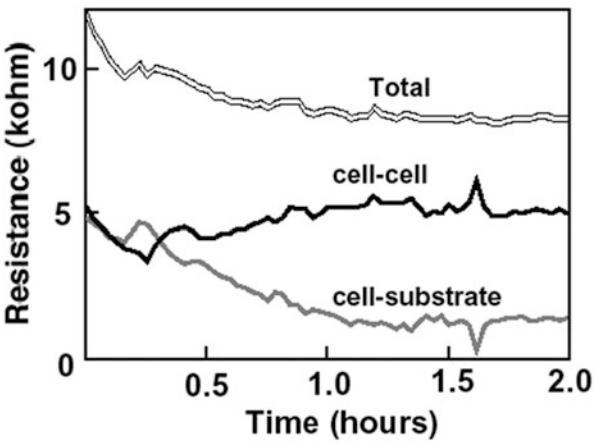

Fig. 8.2 Typical real-time traces of the total (*Double line*), cell-to-substrate (*Gray line*) and cell-to-cell (*Black line*) resistance in the IL-1β stimulated HUVECs

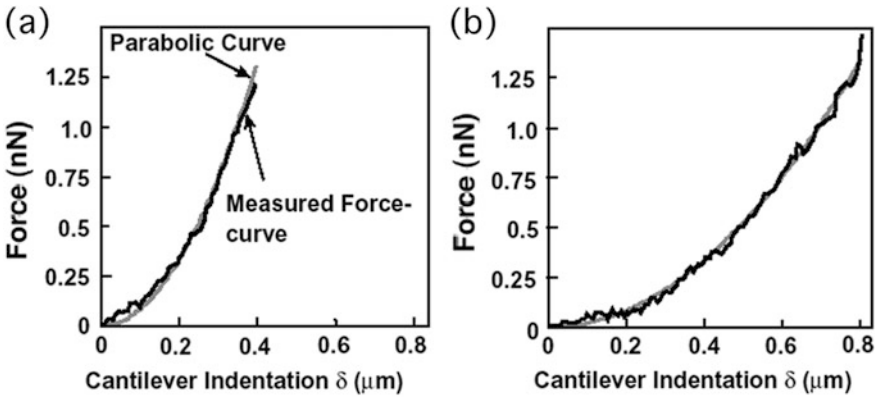

Fig. 8.3 Typical force-curves for the peripheral region of control (**a**) and monocyte adhered (**b**) HUVEC measured with AFM

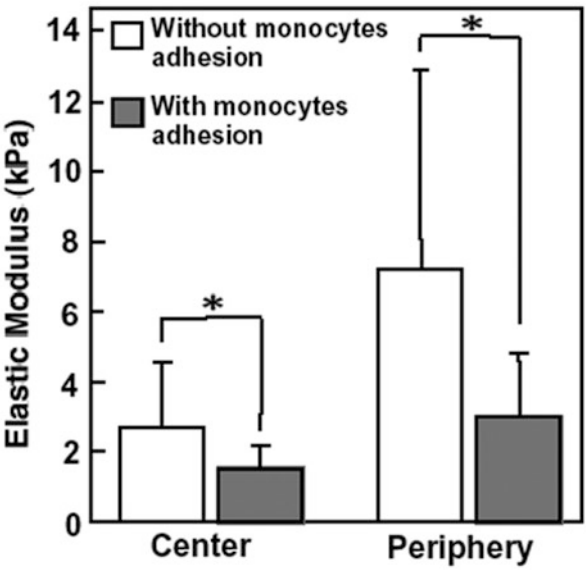

Fig. 8.4 Elastic modulus of HUVECs with and without monocytes adhesion. *$p < 0.05$

Decrease of the endothelial cell-to-substrate resistance (increase of cell-to-substrate gap) is related with the change of the adhesiveness of endothelial cells to the substrate, and the decrease of elastic modulus of endothelial cell indicates the increase of deformability. These may facilitate trans-endothelial migration of monocytes in the later stage.

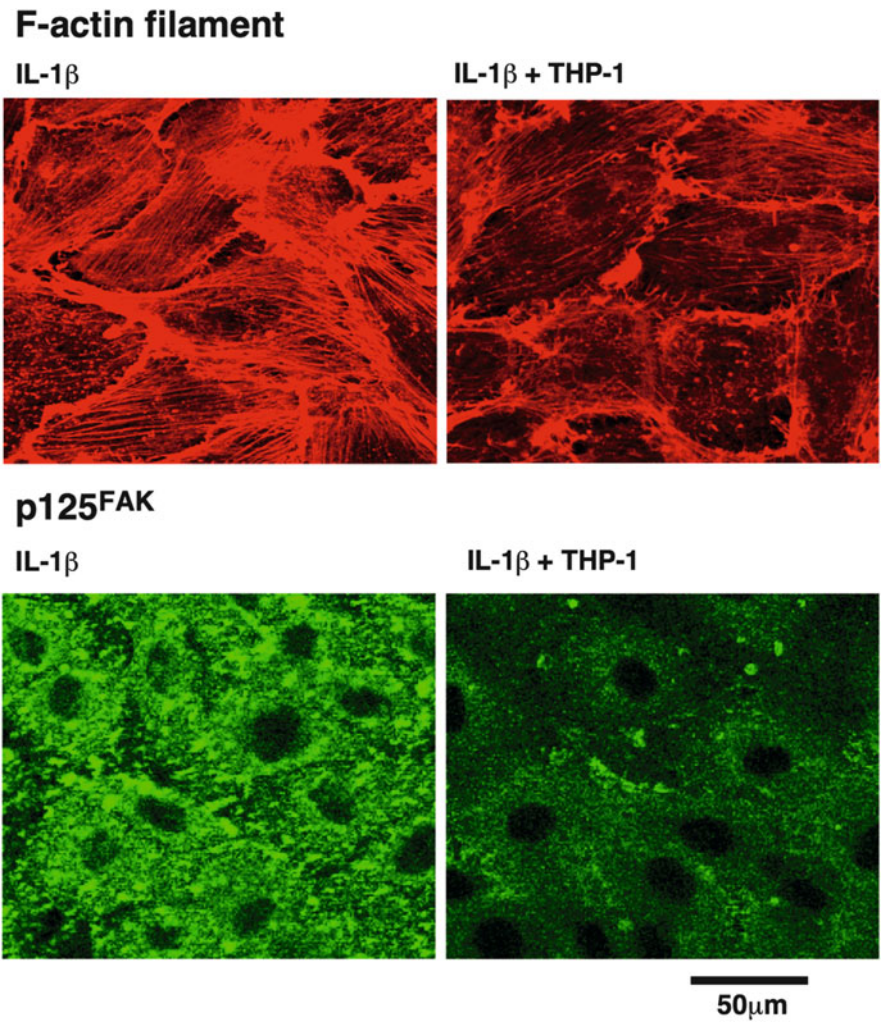

Fig. 8.5 Photomicrographs of F-actin filaments and $p125^{FAK}$ in HUVECs before and after application of THP-1

8.2 Direct Observation of Individual Living Monocytes During Transendothelial Migration

As mentioned above, the transendothelial migration (TEM) of monocytes is the crucial event at the early stage of atherosclerosis. However, considerable part of this complicated process is not well understood, and actually it is not clear how individual living monocytes behave three-dimensionally. We developed an

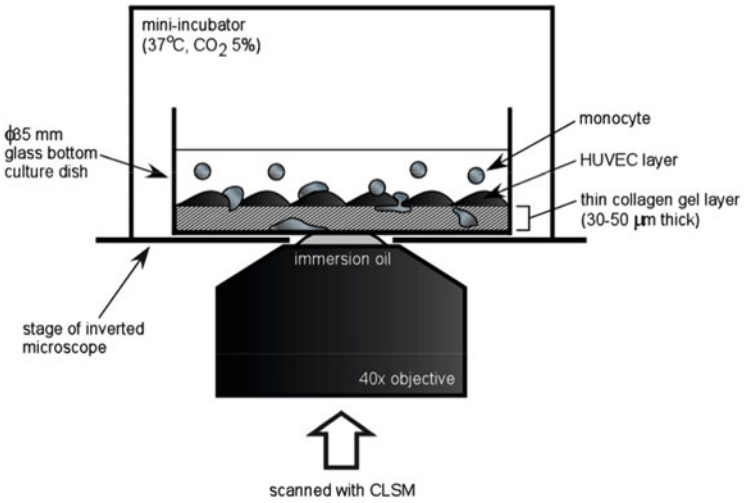

Fig. 8.6 Schematic diagram of newly-developed experimental system. HUVECs were cultured on ultra thin collagen gel layer (30–50 μm thickness) in the glass bottom culture dish. Monocyte behavior on HUVEC monolayer was observed with CLSM using 40 × oil immersion objective

experimental system using confocal laser scanning microscope (CLSM) to analyze and reveal spatiotemporal dynamics of individual living monocytes during TEM (Hashimoto et al. 2004).

Figure 8.6 shows the schematic diagram of the experimental system. Ultra thin collagen gel layer (approximately 30–50 μm thick) was constructed under HUVEC monolayer on glass bottom culture dish to provide both minimal subendothelial space for monocytes to invade, and maximal thickness for focus adjustment of the microscope with high magnification. Before transmigration assay, HUVECs were stained with red fluorescent probe 5-(and-6)chloromethyl SNARF-1, acetate (Molecular Probes, OR), and monocytes were counter-stained with green fluorescent probe CellTracker Green CMFDA (Molecular Probes).

A typical example of time course of TEM is shown in Fig. 8.7. The monocyte started invasion over 3–5 min (arrow) after application on HUVECs, but hesitated to transmigrate, and surprisingly returned onto the apical surface of HUVECs at 7 min (arrow). There were also some other monocytes that had once extended projections into subendothelium, hesitated to transmigrate, retracted them, and started to crawl on HUVECs again. A few minutes later, the monocyte deformed and extended projections into collagen gel again at 12 min ((*) at 12 min). Adhesion of the projection ((*) at 12 min) to collagen gel subsequently caused remained tail of the monocyte ((+) at 12 min) on EC to be retracted into subendothelium over 12–25 min (arrow at 18 and 25 min), and the monocyte completely transmigrated at 30 min (arrow).

We performed quantitative analysis of ratio and time course of TEM of individual monocytes (Table 8.1). Each monocyte at each time point was classified into

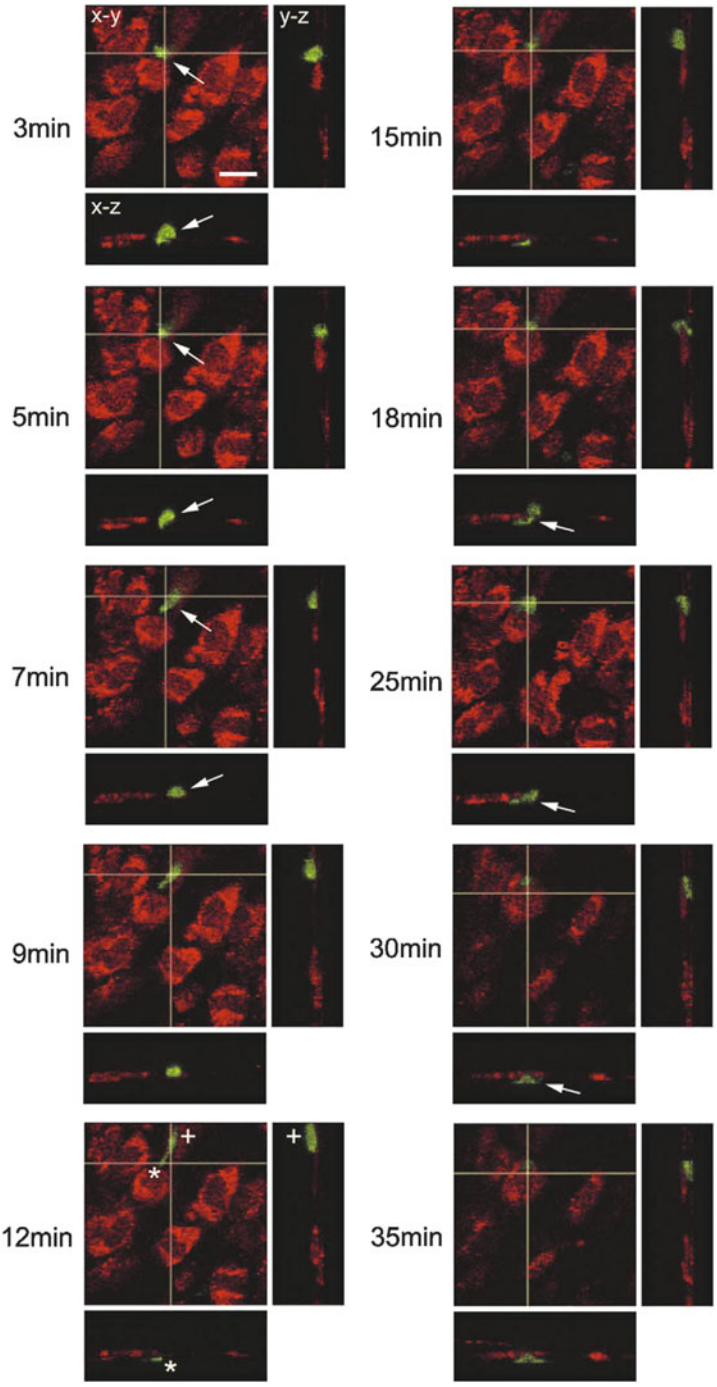

Fig. 8.7 Atypical example of TEM, HUVECs were stained with SNARF-1 (*red*) and monocytes were stained with CellTracker Green (*green*). Bar = 20 μm

Table 8.1 Results of quantitative analysis of ratio and time course of TEM of individual monocytes

	Number of monocytes	**Ratio (%)**
Total adhered monocytes measured (A)	96	—
Monocytes that started invasion (B)	67	69.8 (B/A)
Monocytes that completed transmigration (C)	53	55.2 (C/A)
Ratio (C/B)		79.1 (C/B)
Average time course of TEM		
	Time (min)	**(meant ± SD)**
From adhesion to start invasion (A to B)	8.6 ± 5.4	($n = 61$ monocytes)
From start of invasion to finish of transmigration (B to C)	6.3 ± 3.2	($n = 53$ monocytes)
From adhesion to finish transmigration (A to C)	14 ± 5.2	($n = 47$ monocytes)

three categories according to the stage of TEM, i.e., adhered on endothelium (A), started invasion (B), and completed transmigration (C). Total number of 96 adhered monocytes from five separate culture experiments was measured up to 25–30 min after application on HUVECs. As to ratio of TEM, 67 out of 96 monocytes (69.8 %) started invasion, and 53 out of such 67 monocytes (79.1 %) completely finished transmigration. Times from adhesion (A) to start of invasion (B), from start (B) to finish (C) of invasion, and from adhesion (A) to finish of transmigration (C) were 8.6 ± 5.4 min (mean ± S.D., $n = 61$ monocytes), 6.3 ± 3.2 min (mean ± S.D., $n = 53$ monocytes), and 14 ± 5.2 min (mean ± S.D., $n = 47$ monocytes), respectively.

8.3 Effects of Oxidized LDL on Behavior of Monocytes and Junctional Conformation of Endothelial Cells

It is well known that the accumulation of lipid within the intima is one of principal risk factors for atherosclerosis. In particular, oxidized low density lipoprotein is a crucial factor in atherogenesis. It is also known that monocyte TEM is facilitated by oxLDL (Klouche et al. 1999). However, it is unclear how and at which stage oxLDL promotes monocyte dynamics during multi-step monocyte TEM process. We have investigated the effects of oxLDL on behavior of individual monocyte and junctional conformation of endothelial cells (Hashimoto et al. 2007).

We divided monocyte dynamics into three stages: (1) adhesion on ECs, (2) invasion, and (3) complete transmigration below ECs. Each monocyte at each time was carefully classified into the three stages from 3D-reconstructed images. Figure 8.8a–c shows the representative 3D-cross-sectional images for each stage of monocyte. Migration speed of each monocyte was calculated by tracking the x–y location of the same monocyte temporally in z-projected images (two dimensionally) during

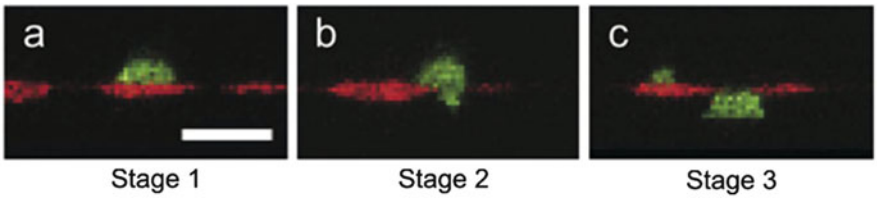

Fig. 8.8 Representative 3D-cross-sectional images at each stage of monocyte (*green*). (**a**) Stage 1: adhesion on ECs (*red*), (**b**) stage 2: invasion and (**c**) stage 3: complete transmigration below ECs. Bar = 20 μm

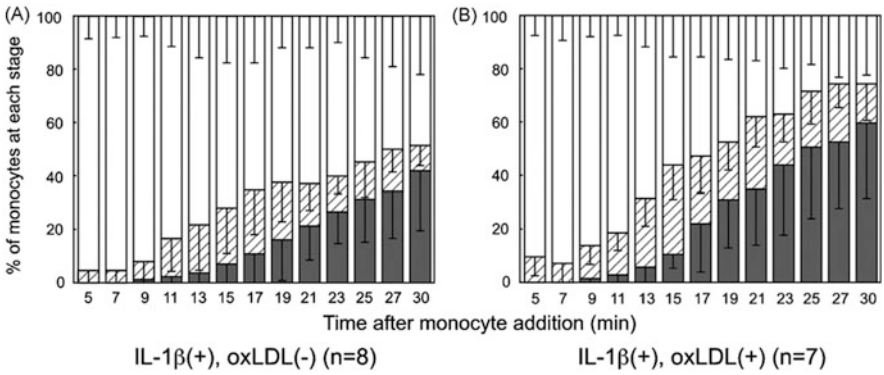

Fig. 8.9 Each monocyte at each time in our TEM assay was classified into three stages (stage 1: *open bars*, stage 2: *hatched bars* and stage 3: *gray bars*; representative images shown in Fig. 8.8) to analyze the detailed temporal kinetics of individual living monocyte. (A) without oxLDL (B) with oxLDL

stage 1 (locomotion on ECs after adhesion before invasion) and 3 (subendothelial migration after invasion).

Using our experimental system described above, detailed analysis in temporal kinetics of individual living monocyte revealed that oxLDL significantly promoted monocyte TEM process (Fig. 8.9a, b). The enhancement of transmigrated monocyte (stage 3) and the reduction of non-transmigrating monocyte (stage 1) by oxLDL were determined to be statistically significant ($p < 0.05$ and $p < 0.004$, respectively) by two-way ANOVA. The temporal change of monocyte population at stage 2 was not statistically significant. OxLDL also enhanced monocyte deformation and spreading to thin, amoeba-like shape.

Initial adhesion of moncoytes to HUVECs (stage 1) significantly increased with IL-1β stimulation as expected. But an additional exposure of subendothelial oxLDL to IL-1β-stimulated HUVECs did not promote the monocyte adhesion further.

To elucidate at which stage oxLDL affects monocyte to promote TEM, we evaluated the stage transition (stage $1 \rightarrow 2$, and $2 \rightarrow 3$) of monocytes by calculating the ratio of monocytes which have reached stage 2 out of the monocytes at stage 1, and stage 3 out of the monocytes at stage 2 in the same living samples. As shown

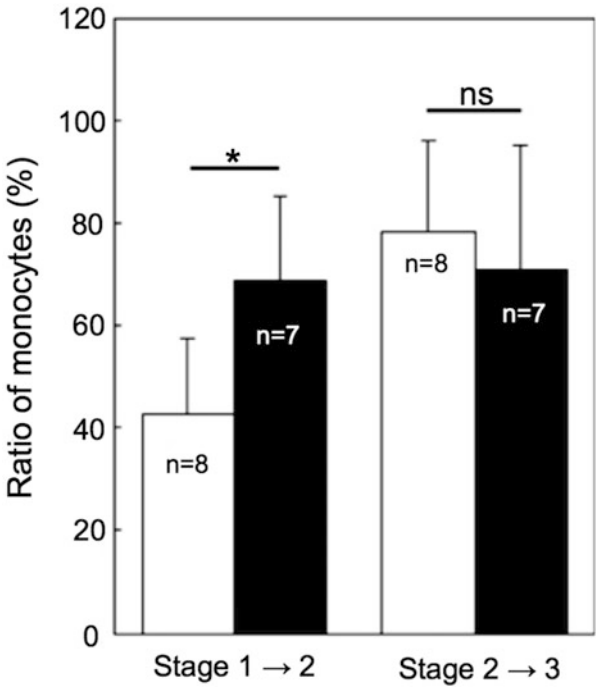

Fig. 8.10 The stage transition of monocytes (stage $1 \rightarrow 2$, and $2 \rightarrow 3$) was evaluated by calculating the ratio of monocytes which have reached stage 2 out of the monocytes at stage 1, and stage 3 out of the monocytes at stage 2 in the same living samples

in Fig. 8.10, oxLDL specifically and significantly increased the ratio of adherent monocytes that started invasion at junctions from stage $1 \rightarrow 2$ (68.7 ± 16.4 % with oxLDL versus 42.9 ± 14.8 % without oxLDL, $p < 0.007$). However, majority of the monocytes (70–80 %) at stage 2 completed transmigration (reached stage 3) regardless of oxLDL, indicating oxLDL has no effect on monocyte transition dynamics once invasion starts (stage2 $\rightarrow$ 3).

To explore the mechanisms of oxLDL-induced stage-specific priming of monocyte (stage $1 \rightarrow 2$), we evaluated the migration speed of monocytes during stage 1 (locomotion on ECs after adhesion before invasion) and 3 (subendothelial migration after invasion). The speed of monocyte was around 3–4 m/min and was not altered by oxLDL in either stage, suggesting that the oxLDL-induced stage-specific priming of monocyte was not the consequence of its enhanced migration speed.

We examined the rearrangements of two major endothelial junctional molecules, PECAM-1 and VEcadherin by oxLDL (without monocyte addition). OxLDL significantly upregulated PECAM-1 and downregulated VEcadherin (Fig. 8.11; 130 %, $p < 0.01$, and 56 %, $p < 0.0002$, respectively, versus control without oxLDL).

OxLDL upregulated PECAM-1 and downregulated VE-cadherin on the intercellular junctions of IL-1β-stimulated HUVECs before monocyte adhesion, which changed junctional conformation to more monocyte acceptable state, and led to the stage-specific promotion of monocyte TEM (stage $1 \rightarrow 2$; the initiation of invasion),

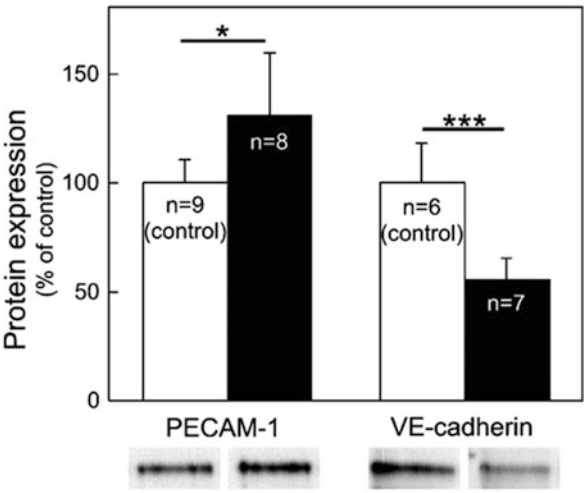

Fig. 8.11 Changes of PECAM-1 and VE-cadherin expression in EC affected with OxLDL. Protein quantifications and corresponding representative images of Western blotting for PECAM-1 and VE-cadherin. OxLDL significantly upregulated PECAM-1 and downregulated VE-cadherin on the intercellular junctions of IL-1β-stimulated ECs without monocyte addition. $*p < 0.01$, $***p < 0.0002$

with no enhancement of its initial adhesion, speeds of locomotion on ECs, or subendothelial migration. Clinically, pharmacological targeting against upregulated PECAM-1 and/or downregulated VE-cadherin could potentially be beneficial with preventing monocyte TEM, which is the key process in early atherogenesis.

8.4 Dynamic Redistribution and Recruitment of Endothelial PECAM-1 at Sites of Monocyte

Leukocytes have been shown to cross EC monolayers by both paracellular (between ECs) and transcellular (through the body of ECs) routes. For paracellular transmigration, many molecules have been reported to be involved, including platelet-endothelial cell adhesion molecule-1 (PECAM-1) (Mamdouh et al. 2003; Schenkel et al. 2002; Su et al. 2002; Muller et al. 1993), vascular endothelial cadherin (VE-cadherin) (Su et al. 2002; Shaw et al. 2001) junctional adhesion molecules (JAMs), (Keiper et al. 2005; Bradfield et al. 2007) inter-cellular adhesion molecule-2 (ICAM-2), (Huang et al. 2006) and CD99 (Schenkel et al. 2002). It is reported that part of cellular PECAM-1 exists in the lateral border recycling compartment (LBRC), which is located below the surface of the cell at the lateral (Mamdouh et al. 2003, 2008) borders in ECs, and PECAM-1 is constitutively recycled between the LBRC and the cell surface. During paracellular diapedesis of monocytes or neutrophils, this recycling PECAM-1-bearing membrane is targeted rapidly and extensively to the site of diapedesis (Mamdouh et al. 2003). This targeted recruitment is mediated by kinesin family molecular motors and normally functioning microtubules (Mamdouh et al. 2008). However, the molecular dynamics of the targeted recruitment of PECAM-1 has not been directly demonstrated in live cells. Moreover, it is currently unclear what triggers the recruitment during a series of

diapedesis processes from rolling to transmigration, as has only been suggested that homophilic PECAM-1-PECAM-1 interactions between leukocytes and ECs are required for the recruitment (Mamdouh et al. 2003). It is also important to examine whether PECAM-1 plays a selective role for paracellular diapedesis or has some undefined roles in transcellular diapedesis.

We constructed a PECAM-1 fusion vector, in which the C-terminal, intracellular tail of the molecule was linked to green fluorescent protein (GFP) and transfected this PECAM-1-GFP vector into HUVECs. We analyzed the molecular dynamics of endothelial PECAM-1 during monocyte paracellular and transcellular diapedesis in three-dimensions, at a single-cell level, in these live HUVECs, which can not be achieved with a conventional end point-type assay using fixed cells (Hashimoto et al. 2012).

8.4.1 Route of Diapedesis and PECAM-1 Gaps

Of a total of 153 diapedesis events analyzed, only 5 % monocytes (7 events) transmigrated 10 by a transcellular route while approximately 95 % took a paracellular route. Of these, 68 % migrated through bicellular junctions and 27 % through multicellular junctions.

A typical example of the 3D-molecular dynamics of PECAM-1 during monocyte diapedesis through a bicellular junction is shown in Fig. 8.12 PECAM-1 staining at a bicellular junction was intact before the monocyte arrived (0 min). The monocyte adhered to the HUVEC at 6 min after the addition of monocytes started to invade the HUVEC monolayer at 14 min, forming a PECAM-1 gap de novo. Local endothelial PECAM-1 redistributed to surround the transmigrating monocyte, as clearly shown in xy, xz, and yz planes (arrows at 14 and 18 min). The migrating front of the monocyte had already reached the base of the HUVEC layer by 18 min.

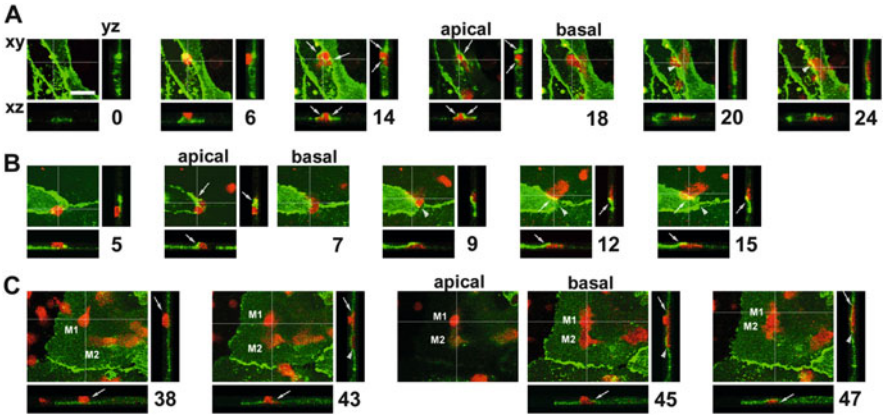

Fig. 8.12 Local redistribution of endothelial PECAM-1 during monocyte transmigration at (A) bicellular (B) multicellular and (C) transcellular

By 20 min, transmigration was virtually complete, but a PECAM-1 gap was still visible, and this had completely resealed by 24 min (arrowheads). Similar dynamics for endothelial PECAM-1 were seen around monocytes migrating through multicellular junctions (Figure 8.12), where gaps formed de novo, with PECAM-1 redistribution at 7–12 min (arrows) and the gap resealing after transmigration at 9–15 min (arrowheads). The majority of these 11 paracellular events were accompanied by PECAM-1 redistribution to surround transmigrating monocytes (77 % for bicellular and 83 % for multicellular junctions). In contrast, Fig. 8.12c shows a monocyte M1 that transmigrated transcellularly, but the redistribution of endothelial PECAM-1 was never observed. At 38 min, M1 was on the apical surface of an HUVEC (arrows), and another monocyte M2 had already transmigrated beneath the HUVEC. At 43–45 min, M2 migrated towards M1, and M1 started to invade the HUVEC transcellularly (arrows) as if attracted by M2, but no redistribution of endothelial PECAM-1 was observed. M1 had almost completed transcellular transmigration by 47 min and appeared to aggregate with M2 (arrows and arrowhead). This mode of transcellular diapedesis, in which adherent monocytes seemed to be attracted by another transmigrated monocyte, was seen in 57 % (4/7) of transcellular events observed in this system. Local recruitment of endothelial PECAM-1 to sites of transmigration after paracellular, but not transcellular diapedesis was observed. A typical example of the 3D molecular dynamics of PECAM-1 after the completion of diapedesis at a bicellular junction is shown in Fig. 8.13a. At 11 min, monocyte M1 was on the apical surface of the HUVEC (arrows). The redistribution of PECAM-1 around M1 was seen during transmigration (arrows and arrowhead at 23 min), as seen in Fig. 8.12a, b. After transmigration, PECAM-1 was dynamically recruited to the site of transmigration to form a PECAM-1 rich region which increased over time (arrowheads at 28–43 min). A similar dynamics of PECAM-1 was seen at multicellular junctions (Fig. 8.13b). At 54–62 min, monocyte M1 invaded the EC layer through a multicellular junction (arrows and arrowheads), and from 62 to 75 min, the recruitment of PECAM-1 to the site of transmigration was seen (arrowheads), as in Fig. 8.13a.

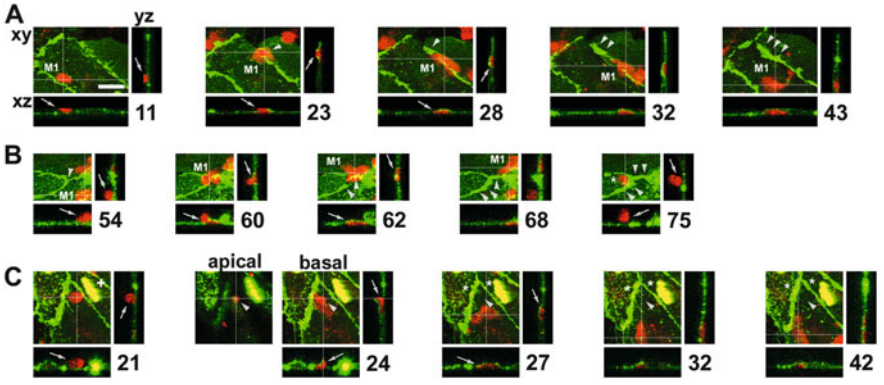

Fig. 8.13 PECAM-1 was recruited to sites of monocytes transmigration at bicellular (**a**) and multicellular (**b**), but not to the transcellular migration site (**c**)

At 75 min, M1 migrated out of 12 sight and another monocyte was observed on the apical surface of HUVEC (* and arrows), but it was not related to the diapedesis of M1. In contrast, PECAM-1 recruitment was never seen to the sites of transcellular diapedesis. Figure 8.13c shows a monocyte that invaded the EC layer transcellularly at 21–27 min (arrows and arrowheads), in which a transcellular pore was clearly visible at 24 min, but endothelial PECAM-1 did not redistribute around the monocyte or was not recruited either to the site of transmigration (arrowhead) or neighboring junctions (*), between 27 and 42 min.

Quantitative image analysis showed a significant, time-dependent increase in PECAM-1-GFP fluorescence specifically at the sites of paracellular transmigration at both bicellular and multicellular junctions. There was up to a 1.4-fold increase within 20 min of transmigration (Fig. 8.14a, b), which was accompanied by a significant reduction in fluorescence in the neighboring cytoplasmic regions (Fig. 8.14c), suggesting that PECAM-1 was recruited from the sub-junctional cytoplasm to the site of transmigration. Fluorescent intensities over the whole scanned area (250 Å ~ 250 μm) remained unchanged (Fig. 8.14c). In contrast, no change in PECAM-1-GFP fluorescence was seen at the sites of transcellular diapedesis (Fig. 8.14b). PECAM-1 recruitment was not seen at bicellular junctions where no transmigration occurred (Fig. 8.14Aa, while many added monocytes had adhered to the HUVEC layer) or in the presence of antibodies against β2-integrin

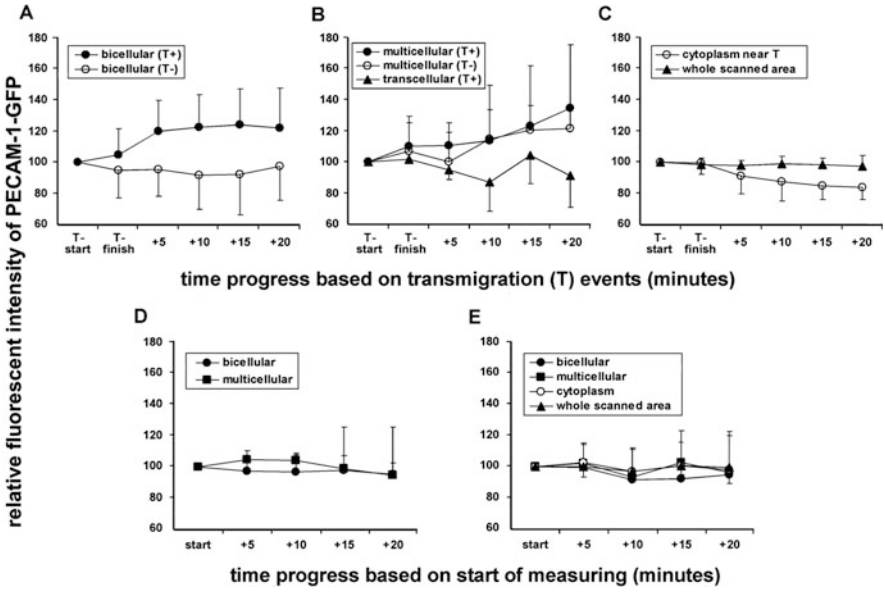

Fig. 8.14 Quantitative image analysis of PECAM-1 recruitment to transmigation sites. (**a**) At bicellular junctions, (**b**) At multicellular junctions, (**c**) PECAM-1-GFP in sub-junctional cytoplasmic regions, (**d**) PECAM-1 recruitment at bicellular ($n = 8$) or multicellular ($n = 6$) junctions when monocyte adhesion was blocked. (**e**) PECAM-1-GFP fluorescence at bicellular junctions ($n = 10$), multicellular junctions ($n = 8$), in the sub-junctional cytoplasmic regions ($n = 10$), or over the whole scanned area ($n = 3$) in control HUVECs without monocytes

and ICAM-1 which blocked monocyte adhesion (Fig. 8.14d), suggesting that the recruitment was driven by monocyte transmigration itself, rather than by adhesion or monocyte-derived soluble factors. At multicellular junctions, the recruitment appeared to occur in the regions where no transmigration occurred (Fig. 8.14b), but not when adhesion was blocked (Fig. 8.14d), suggesting that the recruitment was driven initially by adhesion, and subsequently by transmigration, but not by soluble factors. No changes were observed in any regions in control HUVECs without monocytes (Fig. 8.14e), showing that the recruitment of PECAM-1 was not caused by activities intrinsic to ECs or by artifacts such as photobleaching.

We have presented hear the importance of mechanobiology of endothelial cells and monocyte dynamics in atherogenesis. We have also shown that monocyte adhesion to endothelial cells may facilitate subsequent monocyte transendothelial migration via not only the changes of mechanical properties of EC but also the redistributution of PECAM-1 in EC. It is possible that monocyte adhesion and migration could be mechanical stimulus to endothelial cells, because endothelial cell deformation and/or strain with monocyte adhesion are much more than those by fluid shear stress. To investing the direct effects of monocyte adhesion and/or migration to endothelial cells, the real time observation of F-actin dynamics in endothelial cells and monocytes is needed. Of course, real time observation of signaling molecules in cells also needed. For further investigation, newly designed biomechanical and biophysical experimental technics should be developed.

References

Bradfield PF, Scheiermann C, Nourshargh S, Ody C, Luscinskas FW, Rainger GE, Nash GB, Miljkovic-Licina M, Aurrand-Lions M, Imhof BA (2007) JAM-C regulates unidirectional monocyte transendothelial migration in inflammation. Blood 110:2545–2555

Giaever I, Keese CR (1991) Micromotion of mammalian cells measured electrically. Proc Natl Acad Sci U S A 88:7896–7900

Hashimoto K, Kataoka N, Nakamura E, Asahara H, Ogasawara Y, Tsujioka K, Kajiya F (2004) Direct observation and quantitative analysis of spatiotemporal dynamics of individual living monocytes during transendothelial migration. Atherosclerosis 177:19–27

Hashimoto K, Kataoka N, Nakamura E, Tsujioka K, Kajiya F (2007) Oxidized LDL specifically promotes the initiation of monocyte invasion during transendothelial migration with upregulated PECAM-1 and downregulated VE-cadherin on endothelial junctions. Atherosclerosis 194:e9–e17

Hashimoto K, Kataoka N, Nakamura E, Hagihara K, Okamoto T, Kanouchi H, Mohri S, Tsujioka K, Kajiya F (2012) Live-cell visualization of the trans-cellular mode of monocyte transmigration across the vascular endothelium, and its relationship with endothelial PECAM-1. J Physiol Sci 62(1):63–69

Huang MT, Larbi KY, Scheiermann C, Woodfin A, Gerwin N, Haskard DO, Nourshargh S (2006) ICAM-2 mediates neutrophil transmigration in vivo: evidence for stimulus specificity and a role in PECAM-1-independent transmigration. Blood 107:4721–4727

Kataoka N, Iwaki K, Hashimoto K, Mochizuki S, Ogasawara Y, Sato M, Tsujioka K, Kajiya F (2002) Measurements of endothelial cell-to-cell and cell-to-substrate gaps and micromechanical properties of endothelial cells during monocyte adhesion. Proc Natl Acad Sci U S A 99:15638–15643

Keiper T, Al-Fakhri N, Chavakis E, Athanasopoulos AN, Isermann B, Herzog S, Saffrich R, Hersemeyer K, Bohle RM, Haendeler J, Preissner KT, Santoso S, Chavakis T (2005) The role of junctional adhesion molecule-C (JAM-C) in oxidized LDL-mediated leukocyte recruitment. FASEB J 19:2078–2080

Klouche M, May AE, Hemmes M, Messner M, Kanse SM, Preissner KT, Bhakdi S (1999) Enzymatically modified, nonoxidized LDL induces selective adhesion and transmigration of monocytes and T-lymphocytes through human endothelial cell monolayers. Arterioscler Thromb Vasc Biol 19:784–793

Mamdouh Z, Chen X, Pierini LM, Maxfield FR, Muller WA (2003) Targeted recycling of PECAM from endothelial surface-connected compartments during diapedesis. Nature 421:748–753

Mamdouh Z, Kreitzer GE, Muller WA (2008) Leukocyte transmigration requires kinesin-mediated microtubule-dependent membrane trafficking from the lateral border recycling compartment. J Exp Med 205:951–966

Muller WA, Weigl SA, Deng X, Phillips DM (1993) PECAM-1 is required for transendothelial migration of leukocytes. J Exp Med 178:449–460

Radmacher M, Fritz M, Kacher CM, Cleveland JP, Hansma PK (1996) Measuring the viscoelastic properties of human platelets with the atomic force microscope. Biophys J 70:556–567

Ross R (1993) The pathogenesis of atherosclerosis: a perspective for the 1990s. Nature 362 (6423):801–809

Schenkel AR, Mamdouh Z, Chen X, Liebman RM, Muller WA (2002) CD99 plays a major role in the migration of monocytes through endothelial junctions. Nat Immunol 3:143–150

Shaw SK, Bamba PS, Perkins BN, Luscinskas FW (2001) Real-time imaging of vascular endothelial-cadherin during leukocyte transmigration across endothelium. J Immunol 167:2323–2330

Su WH, Chen HI, Jen CJ (2002) Differential movements of VE-cadherin and PECAM-1 during transmigration of polymorphonuclear leukocytes through human umbilical vein endothelium. Blood 100:3597–3603

Swirski FK, Libby P, Aikawa E, Alcaide P, Luscinskas FW, Weissleder R, Pittet MJ (2007) Ly-6Chi monocytes dominate hypercholesterolemia-associated monocytosis and give rise to macrophages in atheromata. J Clin Invest 117:195–205

Tacke F, Alvarez D, Kaplan TJ, Jakubzick C, Spanbroek R, Llodra J, Garin A, Liu J, Mack M, van Rooijen N, Lira SA, Habenicht AJ, Randolph GJ (2007) Monocyte subsets differentially employ CCR2, CCR5, and CX3CR1 to accumulate within atherosclerotic plaques. J Clin Invest 117:185–194